Cell surface acid-base properties of the cyanobacterium Synechococcus: Influences of nitrogen source, growth phase and N:P ratios

Yuxia Liu, D. S. Alessi, G. W. Owttrim, J. P. L. Kenney, Qixing Zhou, S. V. Lalonde, K. O. Konhauser

Geochimica Et Cosmochimica Acta
August 2016, Volume 187 Pages 179-194
https://doi.org/10.1016/j.gca.2016.05.023
https://archimer.ifremer.fr/doc/00639/75069/

Cell surface acid-base properties of the cyanobacterium Synechococcus: Influences of nitrogen source, growth phase and N:P ratios

Liu Yuxia [1, 2], Alessi D. S. [2], Owttrim G. W. [3], Kenney J. P. L. [4], Zhou Qixing [1, *], Lalonde Stefan [5], Konhauser K. O. [2, *]

[1] Nankai Univ, Coll Environm Sci & Engn, Tianjin 300071, Peoples R China.
[2] Univ Alberta, Dept Earth & Atmospher Sci, Edmonton, AB T6G 2E3, Canada.
[3] Univ Alberta, Dept Biol Sci, Edmonton, AB T6G 2E9, Canada.
[4] Imperial Coll, Dept Earth Sci & Engn, London SW7 2AZ, England.
[5] CNRS, European Inst Marine Studies, Lab Domaines Ocean, UMR6538,UMR 6538, Brest, France.

* Corresponding authors : Qixing Zhou, email address : zhouqx@nankai.edu.cn ; K. O. Konhauser, email address : kurtk@ualberta.ca

Abstract :

The distribution of many trace metals in the oceans is controlled by biological uptake. Recently, Liu et al. (2015) demonstrated the propensity for a marine cyanobacterium to adsorb cadmium from seawater, suggesting that cell surface reactivity might also play an important role in the cycling of metals in the oceans. However, it remains unclear how variations in cyanobacterial growth rates and nutrient supply might affect the chemical properties of their cellular surfaces. In this study we used potentiometric titrations and Fourier Transform Infrared (FT-IR) spectrometry to profile the key metabolic changes and surface chemical responses of a Synechococcus strain, PCC 7002, during different growth regimes. This included testing various nitrogen (N) to phosphorous (P) ratios (both nitrogen and phosphorous dependent), nitrogen sources (nitrate, ammonium and urea) and growth stages (exponential, stationary, and death phase). FT-IR spectroscopy showed that varying the growth substrates on which Synechococcus cells were cultured resulted in differences in either the type or abundance of cellular exudates produced or a change in the cell wall components. Potentiometric titration data were modeled using three distinct proton binding sites, with resulting pKa values for cells of the various growth conditions in the ranges of 4.96-5.51 (pKa(1)), 6.67-7.42 (pKa(2)) and 8.13-9.95 (pKa(3)). According to previous spectroscopic studies, these pKa ranges are consistent with carboxyl, phosphoryl, and amine groups, respectively. Comparisons between the titration data (for the cell surface) and FT-IR spectra (for the average cellular changes) generally indicate (1) that the nitrogen source is a greater determinant of ligand concentration than growth phase, and (2) that phosphorus limitation has a greater impact on Synechococcus cellular and extracellular properties than does nitrogen limitation. Taken together, these techniques indicate that nutritional quality during cell growth can noticeably influence the expression of cell surface ligands and their measurable densities. Given that cell surface charge ultimately affects metal adsorption, our results suggest that the cycling of metals by Synechococcus cells in the oceans may vary regionally.

Keywords : Synechococcus, Marine cyanobacteria, FTIR, Potentiometric titrations, Cell surface reactivity, Nitrogen and phosphate limitation

1. INTRODUCTION

The bacterial cell surface acts as a highly reactive interface due to an abundance of ligands, such as carboxyl, hydroxyl, phosphoryl and amine groups. These ligands are associated with peptidoglycan, teichoic and teichuronic acids on the surfaces of Gram-positive bacteria, and lipopolysaccharides (LPS), phospholipids and proteins on the surfaces of Gram-negative bacteria, such as cyanobacteria (Cox et al., 1999; Borrok et al., 2004). Importantly, they are proton-active and capable of binding a wide variety of metal cations (Fein et al., 1997; Cox et al., 1999; Pradhan et al., 2007; De Philippis et al., 2011), anions (Colica et al., 2010; Kenney et al., 2012) and organic compounds (Baughman et al., 1981; Fein and Delea, 1999; Chen and Wang, 2008) from solution. In turn, these sorbates may serve as sites for the nucleation of authigenic mineral phases (Clarke et al., 1997; Konhauser et al., 1998).

Most bacteria-metal interactions are believed to be mediated by the types and numbers of surface functional groups present on the outer membrane of bacterial cells (Fein et al., 1997; Daughney et al., 2001), as well as the variability in the concentration of some ligand-bearing organic components of the cell wall (e.g., teichoic and teichuronic acids; Beveridge et al., 1982). These variations ultimately arise in response to the growth conditions. Previous investigations revealed that the composition of the culture media, temperature, metabolic pathway, growth phase and pH strongly affected the structural and elemental composition of the bacterial cell wall (Cox et al., 1999; Borrok et al., 2004;

Haas, 2004; Hong and Brown, 2006; Yang et al., 2006). These may impart the cell surface with differing surface chemistry and charge characteristics, which could then influence the microorganism's hydrophobic and hydrophilic properties, adhesive capacities, and further affect the transport and bioremediation of contaminants (e.g., trace metals and organic pollutants) in the subsurface (Fein et al., 1997; Lalonde et al., 2008a; Castro et al., 2010). Growth phase may also impact cell wall composition and ultimately metal uptake by microorganisms. Bruinsma et al. (2001) observed that *Pseudomonas aeruginosa* grown to mid-exponential phase possessed greater concentrations of nitrogen-rich cell surface components and adhered better to hydrophobic and hydrophilic substrata than cells in the early stationary growth phase. Boonaert and Rouxhet (2000) reported that *Lactobacillus helveticus* contained more polysaccharide-rich compounds in stationary phase than during exponential growth. In contrast, other research indicated that bacterial surface compositions remain unchanged in response to growth phase. For example, Haas (2004) reported that growth phase had negligible influence on the ligand distributions of the Gram-negative *Shewanella putrefaciens*, and Jiang et al. (2004) showed that the dominant functional groups on *Pseudomonas stutzeri* cell walls did not change over time with growth. Cumulatively these results suggest the effects of growth phase are species-specific.

As progression through growth phase is dictated, in part, by nutrient concentrations, it is not surprising that variability in cell composition with growth phase may be attributable to the nutrient composition of the growth media. For example, nutrient

limitation, such as P, may specifically reduce acidic functional group sites on bacterial surfaces (Hancock, 1991), and may ultimately impact the physiology and diversity of planktonic organisms in the oceans (Lomas et al., 2014). Previous studies analyzed how the protein and LPS molecule composition of bacteria change as a function of growth stage, and the extent to which these modifications altered the adhesive nature of the cells (Huisman et al., 1996; Bruinsma et al., 2001; Walker et al., 2005). In this context, Malouin et al. (1991) suggested that cell growth in phosphate- or glutamate- enriched media caused an augmentation in major phospholipid species in *Escherichia coli*. Nutrient levels have also been reported to induce changes in the size and shape of bacteria (Borrok et al., 2004), but whether these changes affect the density of functional group sites on bacterial surfaces is unknown. The situation becomes more complex with the consideration of facultative metabolic pathways. For bacteria that are capable of switching amongst multiple metabolic pathways, the presence or absence of specific nutrients may dictate the expression of nutrient specific chelation agents and membrane transport proteins (Wandersman and Delepelaire, 2004; Lalonde et al., 2008a; Swanner et al., 2015).

Fixed nitrogen and phosphorus have been shown to limit biologically mediated carbon assimilation in the oceans (e.g., Howarth, 1988; Tyrrell, 1999). Though the average N:P atomic ratio of the dissolved inorganic nutrients in the oceans is ~14.7, the approximate Redfield ratio (Falkowski, 1997), this value may vary with internal nutrient cycling processes, such as nitrogen fixation and/or denitrification within oceanic oxygen

minimum zones (Deutsch et al., 2012). Previous studies have shown that cell surface N:P ratios are closely related to their electrophoretic properties. For example, Mozes et al. (1988) showed that there was a direct correlation between the cell surface N:P atomic concentration ratio and the cell's electrostatic charge; the presence of phosphate groups mainly determined the anionic surface charges, while nitrogenous groups were linked to increased positive charges. Boonaert and Rouxhet (2000) suggested that the difference in electrokinetic properties between *Lactococcus lactis* and *Lactobacillus helveticus* is related to N:P surface concentration ratios, which reflects the relative exposure of proteins and phosphate groups at the surface. However, there is still a scarcity of information linking the alteration of N:P ratios to changes in bacteria cell wall composition or surface properties.

The relationship between nutrient availability, biomass N:P ratios and cell surface reactivity and charge characteristics is important for understanding how natural marine *Synechococcus* populations might effect metal sorption in different environments, such as nutrient-rich coastal waters versus open ocean oligotrophic waters. In strongly P-limited regions of the ocean, cyanobacteria such as *Prochlorococcus* eschew phospholipids for sulfolipids, dramatically reducing their P requirements and fundamentally altering their cell wall (Van Mooy et al., 2006), and it has been recently suggested that some cyanobacteria may also incorporate Si into their cell walls (Baines et al., 2012). This remarkable degree of cyanobacterial cell wall plasticity reported for the marine realm has remained largely unexplored despite its strong potential importance for biomass surface

reactivity and trace metal adsorption from seawater. Furthermore, while cyanobacteria are ubiquitous in marine waters, their abundance and species distribution in the ocean is highly heterogeneous, with community composition showing clear shifts across coastal to open ocean transects as a function of both macro- and trace-nutrient availability (e.g., Johnson et al., 2006; Ahlgren and Rocap, 2012; Sohm et al., 2016). Given the critical role of cyanobacteria in surface productivity, carbon export and macronutrient cycling, understanding how the physico-chemical surface properties of cyanobacteria vary across ocean-scale environmental gradients is of paramount importance for understanding the full extent of their geochemical impact in the marine realm.

The overall objective of this study was to investigate variations in the chemistry of the combined cell wall and capsular extracellular polymeric substances (EPS) of a *Synechococcus* strain, PCC 7002 (henceforth referred to as *Synechococcus*) in terms of the identity and abundance of extracellular proton-active functional groups. We studied these changes as a function of growth phase (exponential, stationary and death phase), nitrogen metabolisms (nitrate, ammonium and urea) and N:P ratios (N:P ratios that lead to both nitrogen- and phosphorus-limited conditions). *Synechococcus* was chosen because it comprises a significant fraction of the marine plankton (contributing approximately 17% of net primary production; Flombaum et al., 2013), and recently, Liu et al. (2015) suggested that the chemical reactivity of the cyanobacteria's surfaces towards cationic trace elements might be critical to understanding the role that planktonic cyanobacteria play in trace metal sorption from the marine water column.

2. MATERIALS AND METHODS

2.1. Bacterial growth

Cyanobacterial strain *Synechococcus* sp. PCC 7002 (from Dr. Donald Bryant, Penn State University) were grown at 30°C in Medium A (Stevens and Van Baalen, 1973) supplemented with 0.01 M $NaNO_3$ (designated A+ medium; Stevens and Porter, 1980) and buffered with Tris(hydroxymethyl)aminomethane (Tris) buffer (100 g/L) at pH 8.2. Cultures were then acclimated over at least 3 transfers to grow on either nitrate (11.76 mM $NaNO_3$), ammonium (11.76 mM NH_4Cl), or urea (11.76 mM $CO(NH_2)_2$) as the sole nitrogen source. Acclimated cultures were maintained by successive transfer into 50 mL of media with 10% v/v inoculations. Sufficient biomass for potentiometric titrations or FT-IR spectra was obtained by growing three 300 mL cultures, inoculated from the same source culture, and each grown in 1 L Erlenmeyer flasks. Agitation and aeration was provided by constant shaking on a combination incubator-rotary shaker set to 150 rpm, and bubbling with filtered and humidified air (Note: N_2 was not scrubbed, since *Synechococcus* 7002 does not fix N_2). Growth was monitored by measuring optical density at 750 nm (OD_{750}) using a UV-visible spectrometer, and cultures were harvested at absorbance ranges of 0.5 to 0.6, 0.9 to 1.0 and 1.2 to 1.3 for exponential, stationary and death phase cells, respectively. The ranges of resulting *Synechococcus* concentrations, measured using a haemocytometer, are $6.4\sim7.5\times10^{10}$ cells/L, $1.1\sim1.25\times10^{11}$ cells/L and $1.5\sim1.65\times10^{11}$ cells/L for exponential, stationary and death phase, respectively. The

growth rate varied in response to nitrogen source, and therefore, the time of harvest varied for each condition. No significant differences in cell counts were observed amongst the N sources used.

$NaNO_3$ served as the N source and KH_2PO_4 served as the P source. The following five N:P (g:g, mass basis) ratios were tested, where one nutrient was held constant and the other varied above and below the optimum reference condition: (1) N:P = 14.5:1, minimal A+ media reference conditions of 1.0 g $NaNO_3$ and 0.05 g KH_2PO_4 per liter (14.5:1 reference); (2) N:P = 30:1, 2.1 g $NaNO_3$ and 0.05 g KH_2PO_4 per liter (30:1 high $NaNO_3$); (3) N:P = 5:1, 0.35 g $NaNO_3$ and 0.05 g KH_2PO_4 per liter (5:1 low $NaNO_3$); (4) N:P = 30:1, 1.0 g $NaNO_3$ and 0.024 g KH_2PO_4 per liter (30:1 low KH_2PO_4); (5) N:P = 5:1, 1.0 g $NaNO_3$ and 0.14 g KH_2PO_4 per liter (5:1 high KH_2PO_4). Cells were harvested at an OD_{750} of 0.5 to 0.6 during exponential phase. They were then centrifuged at room temperature (14,500 g, 10 min, 30°C), washed four times in 0.01 M $NaNO_3$ electrolyte solution, and incubated for 10 min between washes.

Heat-killed biomass, similarly prepared and harvested with concentrations of biomass equivalent to death phase titrations, were autoclaved at 121°C for 20 min after the final resuspension in the $NaNO_3$ electrolyte solutions. Samples for potentiometric titrations were collected upon cooling to room temperature.

2.2. Fourier Transform Infrared (FT-IR) spectroscopy

FT-IR spectroscopy was used to elucidate the changes in cells or in the composition or

extent of EPS encapsulating the *Synechococcus* cells. Immediately after harvesting and washing four times in 0.01 M $NaNO_3$ electrolyte solution, cells were oven dried at 60^{o}C for 24 h, then mixed with KBr powder (1:50, wt/wt) and pressed into a pellet. FT-IR spectra were collected using a deuterated triglycine sulphate (DTGS) detector attached to a Thermo Nicolet FT-IR Spectrometer 8700. Infrared spectra were acquired using transmission mode through the KBr disk over the range of 4000-500 cm^{-1}, which were transformed to absorbance spectra using the Thermo Scientific OMNIC spectroscopy software package. The spectra were comprised of an average of 128 scans and had a resolution of 4 cm^{-1}. All spectra were corrected for a KBr background. Measurements were carried out in duplicate using two biological replicates. We focus our analyses on the wavenumber region between 1800 and 900 cm^{-1}, as this region contains the most important microbial vibrations (the "double bond" and the "fingerprint" region; Diem, 1993; Benning et al., 2004). In order to compare the spectra collected in our study, all spectra were baseline corrected and area normalized according to Felten et al. (2015).

2.3. Potentiometric titrations

Plastic and glassware used for solution preparation and potentiometric titrations were soaked in 10% v/v nitric acid for 24 h and subsequently soaked in sterile 18 MΩ water for 48 h. Titration suspensions were prepared by adding 0.5-0.7 g of biomass (wet weight after washing) to approximately 50 g of electrolyte solution (0.01 M $NaNO_3$) (exactly weighed in each instance) in a titration flask. The flask was fitted with a double-junction

glass pH electrode (Orion ROSS ultra, filled with 3 M KCl) which was calibrated using commercial pH buffers (Thermo Fisher Scientific; pH 2.0, 3.0, 4.0, 7.0, 10.0), as well as a thermocouple, magnetic stir bar, bubbler, and titrant dispenser. The suspension was acidified with 2 M HCl to a pH of 3.0, sealed with Parafilm, and allowed to equilibrate for 30 min under a constant purge of Argon (Ar) gas.

Titrations were performed alkalimetrically from pH approximately 3.0 to 11.1 using a Man-Tech Associates QC-Titrate autotitrator that variably delivered CO_2-free 0.01 M NaOH. pH resolution was set to 0.1 and electrode stability criteria <0.1 mV/s for each step. A typical titration took approximately 50 min. Once pH 11.1 was achieved, reverse 'down-pH' titrations were performed, decreasing the suspension to pH 3 with aliquots of 0.01 M HCl in order to test the reversibility of proton binding on the cell surfaces. Cellular integrity was assessed before and after the titrations by autofluorescence using a Zeiss Axioskop 2 epifluorescence light microscope (red-type reflector slide). Cells that lyse may appear intact, but do not display autofluorescence. No significant change in the relative abundance of cells that displayed autofluorescence was noted after the titration procedure. When comparing cell counts between brightfield microscopy and epifluorescence, identical trends were observed. Immediately following titration, biomass was filtered onto preweighed Whatman GF/C #42 filters (0.45 μm) and oven dried at 65^{o}C for 48 h for dry weight determination. Titrations were carried out in triplicate using three biological replicates. Blank titrations were performed for machine calibration, using bacteria-free 0.01 M $NaNO_3$ electrolyte solutions only.

To determine the acidity constants (expressed as pKa, equivalent to –log Ka) and concentrations of proton active functional groups on the bacterial surfaces, a non-electrostatic surface complexation model, using the FITEQL 4.0 software program, was employed to fit the potentiometric titration data (Westall, 1982; Herbelin and Westall, 1999). The charge balance in each titration step was calculated by using:

$$[C_a - C_b] = [-Q] + [H^+] - [OH^-] \quad (1)$$

where $[C_a - C_b]$ is the concentration of acid added minus the concentration of base added, $[H^+]$ and $[OH^-]$ are the concentrations of proton and hydroxyl ions, respectively, and $[-Q]$ is the negative charge excess owing to deprotonation of bacterial ligands in solution, normalized per gram of biomass.

All bacteria samples showed measureable buffering capacity over the investigated pH range (pH 4-10) of this study. The proton adsorption reactions responsible for buffering were reversible on the time scale of these experiments (reversibility tested by forward and back titrations; Figure S1). Three-site (pKa) non-electrostatic models were developed to describe the proton reactivity of each bacterial condition using the FITEQL 4.0 program (Herbelin and Westall, 1999). Three sites were chosen because the variance value, V(Y), of these models indicated good fits to the data (Table 2 & 5; $0.1 < V(Y) < 20$), and secondly to keep consistency with the study of Liu et al. (2015). Figure 3 & 4 and Table 2 & 5 summarized the composite FITEQL model results for titrations involving all of the growth conditions examined in this study.

2.4. Statistical analyses.

The Tukey-Kramer test in conjunction with one-way Analysis of Variance (ANOVA) was employed to compare means of paired samples, and the ability for the mean values to describe each condition investigated. All statistical tests were performed at significance levels of 0.05 and 0.1 (Lalonde et al., 2008a, b). Confidence intervals greater than 0.95 indicate statistically significant similarity, while confidence intervals less than 0.05 and 0.1 indicate statistically significant difference.

3. RESULTS

3.1. FT-IR spectra of bacteria samples

Synechococcus cells were harvested from cultures grown with different nitrogen sources ($NaNO_3$, NH_4Cl, and urea) at different stages of growth (exponential phase, stationary phase, and death phase) and different N:P ratios. Bacterial cells were analyzed using FT-IR spectroscopy and the resulting spectra are displayed in Figure 1 (1A: three nitrogen sources at exponential phase; 1B: three nitrogen sources at stationary phase; 1C: three nitrogen sources at death phase; as duplicate FT-IR spectra are similar, data from one of two replicates is presented) and Figure 2 (varying N:P ratios). The proposed band assignments are presented in Table 1.

Irrespective of the incubation time and the contents of the growth media, the FT-IR spectra collected for *Synechococccus* cells were relatively similar to each other and consistent with those obtained by other studies examining bacterial cells and proteins

(after Zeroual et al., 1994; Kansiz et al., 1999; Benning et al., 2004; Jiang et al., 2004; Omoike and Chorover, 2004; Yee et al., 2004; Dittrich and Sibler, 2005; Kong and Yu, 2007; Leone et al., 2007; Meade et al., 2007; Movasaghi et al., 2008; Castro et al., 2010; Quilès et al., 2010; Alessi et al., 2014).

Figure 1 shows how cells were affected by changes in nitrogen source and growth phase. Differences between various growth phases were minimal, with most changes occurring in the Amide I, II, and III and carbohydrate regions of the spectra. Changes in the Amide I band may be due to changes in the concentrations of water or water vapor in the samples, or may be due to changes in the production of proteins or carboxylic acids, while changes in the Amide II and III bands resulted from changes in N-H and C-N groups of the proteins. In some cases the nitrogen source for some growth phases greatly affected the cells.

Cells in exponential growth phase (Figure 1A) showed significant changes in the amide I, II, and III regions for proteins, as well as in peaks at 1105 and 1080 cm^{-1} that represent carbohydrates and phosphodiesters, respectively. When cells were grown using urea as the nitrogen source, there was a decrease with respect to cells grown in NH_4Cl and $NaNO_3$ in the amide I peak and an increase in peaks in the 1105 and 1080 cm^{-1} region. This either means that there is a change in the type of phospholipids produced under these growth conditions, or the very sharp nature of this peak may indicate that the material may be more crystalline, and therefore, may be a relic of the sample preparation and relate to some residual media in the sample which crystallized upon drying. When

cells were grown on $NaNO_3$ there was a shift in the amide II peak towards lower wavenumbers, which is likely due to a change in the relative intensities of the N-H to the C-N groups in the amide II region. This may relate to the production of different amino acids during exponential phase of growth when $NaNO_3$ is the N-source. It is important to note that in stationary and death phase, the same shift in the amide II band observed when the cells at exponential growth phase are grown on $NaNO_3$ is present. Therefore, the same amino acids produced in exponential growth phase grown on $NaNO_3$ are present throughout all further growth stages despite changing N-sources.

Cells harvested at stationary phase (Figure 1B) exhibited the same trend in the amide I region as the cells in exponential growth. However, in stationary growth phase the other significant differences were in the amide II, amide III and in the carboxylic groups represented by bands c, e, and f, respectively. In the case of amide II, the cells grown on urea showed a decrease in the amount of proteins being produced and an increase in carboxylic groups and an increase in the amide III region. The amide II region consists of 60% N-H bending and 40% C-N stretching. The amide III region consists of 30% C-N stretching, 30% N-H bending, 10% C=O stretching, 10% O=C-N bending and 20% other (Stuart, 1997). Therefore the increase in the amide III peak without a subsequent increase in amide II must represent an increase in C=O stretching. This is in agreement with a similar increase in the band e, representing an increase in carboxylic groups. This may infer that there is a shift to a production of amino acids with a higher ratio of carboxylic acid groups to CH_3/CH_2 groups, such as alanine which is an amino acid used in the

biosynthesis of proteins.

The death phase cells showed similar features when cells were grown on $NaNO_3$ and NH_4Cl, with those cells featuring increased production of polysaccharides, phosphorylated polysaccharides, or phospholipids (Quilès et al., 2010) when compared to those cells grown on urea (Figure 1C). The bands h, j, k and l were enhanced compared to those of urea as well as what was observed for cells at exponential and stationary phase. This indicates that in death phase there is a significant increase in the amount of EPS produced. In addition, there is a shift in band k to lower wavenumbers (1026 cm^{-1}), which suggests that either there is a shift from the type of polysaccharide produced in death phase or that there are more polysaccharides produced to mask the lipids and phosphate-rich molecules in the cell wall. Those grown on urea, however, showed an increased amount of proteins, as reflected by an increase in the bands represented by amide I, II, and III. This is contrary to what was seen in the exponential and stationary phases. There are minor changes in the peak at 1370 cm^{-1} (not identified with a lettered band in the figure, between e and f) indicating that there may be some sporulation, as was reported by Schuster et al. (1999) with changes in nutrient sources. However, it is more likely that these relate to the production of carboxylic acids.

The results indicate that at different growth stages, cyanobacteria are able to process nitrogen sources differently, resulting in differences in their capsular EPS or possibly cell wall structure. These findings correlate well with those of Lalonde et al. (2008a) who similarly observed variability in site distribution of the filamentous, nitrogen fixing

cyanobacterium *Anabaena* sp. PCC strain 7120 when grown under different nitrogen assimilation pathways.

Differences in the FT-IR spectra were also observed in response to manipulation of the N:P ratio (Figure 2). FT-IR spectra from *Synechococcus* cells grown in A+ media with $NaNO_3$:KH_2PO_4 = 14.5:1, representative of the average N:P ratio in seawater, and harvested in exponential phase were used as a standard spectrum in order to be able to compare with the previous results of Liu et al. (2015). The standard spectrum shows the highest proportions of protein production in the amide I and II regions and the lowest proportions of polysaccharide production of all the N:P ratios studied, with the exception of N:P=5:1 (low) which had slightly higher absorbance in the amide II region. Not only is there an increase in the abundance of polysaccharides in all cases where there is a change from the reference N:P ratio, but there is a change in the types of polysaccharides being produced. This can be seen in the change in the peak ratio of the peak at 1080 cm^{-1} (j) to 1048 cm^{-1} (k), where the peak at 1048 cm^{-1} grows with respect to that at 1080 cm^{-1}.

When P is kept constant and N is varied (N:P=30:1 high, N:P=14.5:1 ref, and N:P=5:1 low, where P= 0.05 g and N= 2.1, 1, and 0.35 g, respectively), both reducing and increasing the N content from the reference N:P ratio caused an increase in the presence of carboxyl groups. It also leads to an increase in the production of carbohydrates or nucleic acids, as indicated by an increase in the absorbance at peaks at j, k, and l. When N was the lowest, e.g., N:P=5:1 (low), there was also a significant increase in the absorption in the amide II and III bands, but no corresponding increase in the amide I band. This

means that N-H and C-H groups were increased in that system independently of protein production and, therefore, likely related to the production of fatty acids. When N is kept constant and P is varied, e.g., N:P=30:1 (low), N:P=14.5:1 (ref), and N:P=5:1 (high), where N=1 g and P= 0.024, 0.05, and 0.14 g, respectively, the bands followed a similar pattern as when P was fixed. The exception is when N was fixed there were more polysaccharides and less protein produced.

In general, as the system moves away from the ideal N:P ratio, there is an increase in C-O groups and a decrease in N-H, C-N groups. There is no general increase in P=O groups, because no change in the corresponding peak at band g is observed. Given that the standard N:P spectrum has the highest absorbance at the Amide I band (proteins) and the lowest absorbance in the polysaccharide region, this indicates that the average seawater N:P ratio promotes the production of proteins. However, if this ratio changes, whether because of a greater or lower N:P ratio, there is a shift in the cells to produce more polysaccharides.

3.2. Potentiometric titrations

3.2.1. Nitrogen sources and growth phases

Synechococcus cells grown under the growth conditions tested here have pKa values in the range of 4.96-5.51 (pKa_1), 6.67-7.42 (pKa_2) and 8.13-9.95 (pKa_3) (Table 2). Based on spectroscopic studies of cell walls and metal binding to cells (e.g., Sarret et al., 1998; Hennig et al., 2001; Boyanov et al., 2003; Benning et al., 2004; Dittrich and Sibler, 2005),

and analogy in acidity constants with respect to known compounds, the first group of acidic proton binding sites with pKa values in the range of 4.96-5.51 can be attributed to carboxylic groups (pKa = 2 to 6); the second group having pKa values of 6.67-7.42 to phosphoryl groups (pKa = 5.65 to 7.5); and the most basic pKa range of 8.13-9.95 to amine groups (pKa = 8.0 to 10.6) (Jiang et al., 2004; Konhauser, 2007; Castro et al., 2010). The total site concentration (N_{tot}) of *Synechococcus* cells, normalized to the dry weight of bacteria present, was in the range of 17.61 - 34.18 mmol/g (Table 2) under the experimental conditions tested.

In order to assess reproducibility, three replicate titrations of each condition were performed and modeled independently. The average error on pKa distributions within a condition is generally less than 1%: carboxyl (0.02-0.09%); phosphoryl (0.02-0.19%); and amine ligands (0.09-0.30%) (Table 2). Larger inter-experimental error is observed in predicted site densities. Modeled carboxyl site densities vary by 0.16-1.10%; phosphoryl site densities vary by 0.20-0.62%; and amine site densities vary by 0.14-1.60% (Table 2). Sources of error inherent to the experimental method, such as weighing the bacteria and preparation procedure, may contribute to variation observed in pKa values and site densities. Generally, model pKa values and site densities are highly reproducible amongst the three individual titrations (of independently grown cultures) for each of the growth conditions. We suggest that variations among different growth conditions are related to alterations in surface properties of the individual cultures of the bacteria.

The majority of site abundance parameters for nitrate assimilation are different from

those of either ammonium- or urea-assimilated populations (Table 2). The model results vary with growth phase even within one nitrogen metabolic pathway. Irrespective of growth phase, *Synechococcus* cells grown on ammonium and urea assimilation pathways show lower total ligand densities relative to the nitrate assimilation pathway (approximately 20-27%, 15-33%, and 19-26% lower for exponential (Exp.), stationary (Stat.) and death (Dec.) growth phase, respectively) (Table 2). The most significant changes are related to phosphoryl for ammonium assimilation and are related to amine for urea assimilation (Table 2). Concomitantly, the pKa values (pKa_1, pKa_2, and pKa_3) calculated in FITEQL are systematically lower for urea assimilation than the nitrate and ammonium assimilation pathways, and the trend is especially true at the early growth stage (exponential and stationary phase; Table 2).

With respect to growth phase, the total ligand concentrations of nitrate grown cells are negatively correlated with growth stage, with amine groups being the most impacted, as well as a significant shift of pKa_3 to lower pH (Table 2 and Figure 3A). Unlike in nitrate grown cultures, the site densities (carboxyl, phosphoryl and amine) remain stable from exponential to stationary growth phase for ammonium-grown cells, but decrease dramatically in death phase (Table 2 and Figure 3B). For urea grown cultures, though no significant alterations in site concentrations are observed in response to growth phase, site protonation constants (pKa_2 and pKa_3) shift to more acidic pH values from exponential to stationary phase (Table 2 and Figure 3C).

Tukey-Kramer analysis was performed for each class of ligand densities and total

ligand densities, and for each class of ligand pKa values. Differences for all pair-wise comparisons are presented in Table 3 and 4 (Table 3 for site density and Table 4 for pKa value; confidence for Tukey analysis are showing in Table S2 and S3). From comparisons between nitrogen metabolisms, it is apparent that variability in total site concentration occurred, which was accompanied by variability in individual ligand classes (phosphoryl for nitrate vs. ammonium and amine for nitrate vs. urea assimilation pathway; Table 3). Comparisons between growth phases indicate differences in ligand distributions between pKa_3 classes for nitrate assimilation conditions and both pKa_2 and pKa_3 for urea assimilation conditions (Table 4). As a redistribution of ligands between pKa classes may not affect ligand concentration, it would appear that growth phase induced a redistribution of ligands in pKa space with less effect on ligand concentrations. We conclude that for *Synechococcus*, nitrogen metabolism is a greater determinant of ligand concentration than growth phase. A similar conclusion was reached by Hass (2004) for *Shewanella putrefaciens* and Lalonde (2008a) for *Anabaena* sp. PCC 7120.

3.2.2. N:P ratios

Table 5 and Figure 4 depict the impact of N:P ratios on *Synechococcus* cell surface ligand concentrations and pKa values, respectively. Generally, *Synechococcus* cells grown in solutions of N:P = 14.5:1 (the reference condition) yield the highest surface functional group concentrations. Both increasing and decreasing N:P ratios lower the site abundances, especially by a decline of amine site (Table 5 and Figure 4A and 4B). As the

N:P ratio decreased in the two 5:1 conditions, by fixing the concentration of either KH_2PO_4 or $NaNO_3$ to the reference condition and adjusting the other correspondingly, there are measurable shifts in pKa_2 and pKa_3 to lower values (Table 5 and Figure 4A and 4B). Total site concentration between the two 5:1 conditions are similar, but both are dramatically lower than the 14.5:1 reference condition as mentioned above. As the N:P ratio increased to 30:1, similar shifts in pKa_2 and pKa_3 are observed as in the 5:1 experiments (Table 5 and Figure 4A and 4B). Unlike the lower N:P ratios, cultures at the 30:1 ratio that were grown with low KH_2PO_4 exhibit lower site densities than those grown in high $NaNO_3$ at the same ratio, especially for carboxyl and phosphoryl sites (Table 5 and Figure 4A and 4B).

When holding P concentration constant and changing N concentration (Figure 4A: N:P=30:1 vs. N:P=5:1), site pKas and associated site concentrations remain relatively unchanged. However, alteration of P concentration (Figure 4B: N:P=30:1 vs. N:P=5:1) leads to shifts in pKa_2 and pKa_3 to more acidic pH and increased total site concentrations (Table 5 and Figure 4B).

Differences for all pair-wise comparisons are presented in Table 6 and 7 (Table 6 for site density and Table 7 for pKa value; confidence for Tukey analysis are showing in Table S4 and S5). Confidence is generally poor between the reference condition and varying N:P ratios (both increase and decrease), with amine groups being the most affected. Comparison between varying N concentration conditions (holding P concentration constant and changing N concentration) indicate high similarity, while the

lower comparison confidences between varying P concentrations (N:P=5:1 high KH_2PO_4 versus N:P=30:1 low KH_2PO_4 systems) indicate differences in total site densities and pKa distributions. It appears that under the conditions of these batch experiments, phosphorus limitation has a greater impact on *Synechococcus* cell surface properties than does nitrogen limitation.

3.3. Titrations of steam-sterilized cells (inactivated cells)

Steam-sterilized cells were prepared and washed in the same manner as all other experiments following its growth and harvesting, autoclaved, and titrated upon cooling to room temperature. This was done with the intent of lysing cells and releasing all cytoplasmic contents into solution, as well as fully exposing membranes. By this way, it is possible to retain soluble cytosolic contents and evaluate the biomass as a whole for differences in proton reactivity attributable to metabolic pathway. Further to determine whether the differences in reactivity attributed here to growth conditions might be reflected in the cytoplasmic contents (i.e., in the intracellular pools of organic and inorganic compounds; Lalonde et al., 2008a). Heat-killed preparations likely differ in terms of factors such as surface area and soluble biomass components, and these changes would then have contributed excess charge relative to the other titrations presented (Lalonde et al., 2008a, b). As a result, the numerical data from the heat-killed titrations has the sole purpose of testing whether microbial biomass undergoes changes in acid-base behavior as the result of different growth conditions (which a key objective of

this study).

Figure 3 and Table 2 show that the autoclaved lysates provide a 10-20% increase in buffering capacity relative to intact cells for all the nitrogen conditions tested. This is to be expected as cytoplasmic contents, including both organic (e.g., cytosolic proteins, carbohydrates, nucleic acids) and inorganic (e.g., intracellular NH_4^+ and HCO_3^-) components, possess functional groups that have the potential to deprotonate over the range of pH tested in the potentiometric titrations. Overall, cells grown by assimilatory nitrate reduction display ligand concentrations that are higher than those grown on either ammonium or urea sources. Variation in the intracellular pools of organic compounds may be partially responsible for the variations. For example, the cyanobacterium *Synechocystis* sp. strain PCC 6803 has been shown to increase intracellular glutamine concentrations by 30- to 40- fold within seconds of exposure to ammonium, although levels return to normal within approximately 30 minutes (Mérida et al., 1991). This implies that the reduced ligand concentrations inferred for the live nitrate-reducing cultures are a byproduct of cell wall compositional changes associated with growth by that metabolism.

4. DISCUSSION

We examined the effect of nitrogen source, growth phase and N:P ratios on the cell surface properties and composition of the marine cyanobacterium, *Synechococcus*. In

natural and engineered aqueous environments, the source and concentration of nutrition can fluctuate significantly, leading to differing bacterial growth and assimilation conditions. Our experimental results indicate that the magnitude of variability in site concentrations is significantly greater than changes observed for acidity constant (pKa) values corresponding to those sites, suggesting that site identities remain essentially unchanged, while site abundances change in accordance to changing environmental conditions. In other words, while the cells do not produce different polysaccharides, the abundance of those existing polysaccharides changes. This conclusion is in agreement with FT-IR spectra findings presented above, as the intensity and position of band k shifted to lower wavenumber (1026 cm^{-1}) associated with νC-O-C bonds characteristic of polysaccharides in death phase.

FT-IR spectra of bacterial samples can provide insight into the biochemical composition of the cells (e.g., Jiang et al., 2004), and when combined with pKa values from the modeling of titration data and previous spectroscopic studies (see above), allow for tentative identification of the functional groups responsible for cell surface charge. Variations between FT-IR spectra and surface ligand properties from potentiometric titrations are expected to be correlated because the cell wall constitutes 60-70% of total cell weight in a hydrated state (van der Mei et al., 2000). Figure 1 and 2, in conjunction with work done by Jiang et al. (2004), demonstrate that structural transformations and differences occurred in the *Synechococcus* cells under tested experimental growth conditions. With increasing growth stage, there are differences in the protein (amine) and

carbohydrate (1155, 1080, and 1048 cm^{-1}) regions which indicate the production of carboxylic acids and phosphorylated polysaccharides for cells grown on nitrate and ammonium. This is in agreement with variations observed by potentiometric titrations, as the concentration of carboxyl and amine groups vary dramatically from exponential to death phase (Figure 3A and 3B, Table 2). Similar trends were observed by Haas (2004) for *Shewanella putrefaciens*, Bruinsma et al. (2001) for *Pseudomonas aeruginosa* and Ede et al. (2004) for *Bacillus stearothermophilus*. It is possible that ligand concentrations are increased during the exponential growth phase to facilitate the acquisition of nutrients, and are decreased for stationary and death phase cells to minimize interactions with toxic metabolites, or by the fact the cells are no longer metabolically active (Lalonde et al., 2008a). Another possibility is that bacteria will tend to initiate the production of reserve polymers, such as polysaccharides, polyphosphate and nutrient acquisition proteins, at longer incubation times and under nutrient limiting conditions (Borrok et al., 2004; Haas, 2004; Madigan et al., 2008), but continuous nutrient deprivation will tend to limit the number and size of bacteria cells. Thus, although each individual cell, because it is smaller, would have a lower number of sites, it may exhibit a higher site density per gram of biomass due to a higher surface area to mass ratio.

When grown on different nitrogen sources, there were large variations in production of proteins (amine), polysaccharides and LPS for some growth phases. The nitrate medium seems to provide *Synechococcus* cells better growth conditions (most abundant site density) relative to ammonium and urea. Our experiments were based on equivalent

levels of total nitrogen within a molecule. The results suggest that the primary cause of these changes was the presence of urea, and to a lesser extent ammonium, as the sole fixed nitrogen source. Nitrogen utilization by cyanobacteria has been widely studied in the past (Moore et al., 2002; Collier et al. 2012), and altered gene expression in response to nitrogen utilization has been previously described (Hettero et al., 2001; Foster et al., 2007). For instance, Sakamoto et al. (1999) suggested that the expression of both *nrtP* and *narB* genes that encode for nitrate/nitrite permease and nitrate reductase, respectively, in *Synechococcus* strain PCC 7002 are high in nitrate-containing media and low in media containing ammonium or urea. It is, therefore, likely that the cell surface changes observed here result from similarly identified changes in gene expression.

Both increasing and decreasing N:P ratios led to higher proportions of fatty acids, lipids and polysaccharides, as shown in Figure 2. Unlike the FT-IR spectra, our potentiometric titration results indicate constant or lower carboxyl and phosphoryl site concentrations at N:P ratios both higher and lower than the reference condition (14.5:1). This might result from limited nutrition that tends to initiate the production of reserve polymers such as polysaccharides, but also tends to limit the number and size of bacteria cells. FT-IR spectra also exhibit a decrease in the amine bands away from the reference condition, which is in agreement with models of the potentiometric titrations that show a large drop in amine site concentrations at N:P ratios outside of the reference condition.

Regardless of the growth phase and available nutrients, the dominant ionic species exposed on the outer surfaces of *Synechococcus* cells are composed of a combination of

protein and LPS-associated functional groups. Similar results have been reported previously for other cyanobacterial species (e.g., Kansiz et al., 1999; Acharya et al., 2009). *Synechococcus* are substantially anionic during both growth and after lysis, as the amount of negatively charged carboxyl-binding and phosphoryl-binding sites are always greater than positively charged amino-binding sites. The reduction in LPS (associating carboxylic- and phosphoryl- binding sites) could be either a primary effect due to a decreased growth rate, or a secondary effect triggered by an altered cell wall.

We observe that the rearrangement of carbohydrates and LPS (carboxylic- and phosphoryl- binding sites) generally takes place at late growth stages (death phase), while lipid and protein modifications (amine-binding sites) generally occurs in poor nutritional solutions (both increasing and decreasing N:P ratios, as well as most of the ammonium and urea growing cultures). These alterations, in turn, impart the cell surface with different physicochemical properties, such as membrane fluidity, hydrophobicity, and surface charge. Our findings are consistent with previous studies; for instance, Castro and Tufenkji (2007) observed enhanced cell attachment following extended exposure to the nutrient-deprived environment for two *E.coli* strains, while Daughney et al. (2001) showed that *B. subtilis* cells in stationary growth phase adsorbed roughly 5-10% less metal (per unit weight) than those in the exponential growth phase, and roughly 10-20% more metal than sporulated cells.

Overall, these findings indicate that bacteria undergo progressive changes with the relative quality of nutrient solutions through the course of batch cultivation and growth

stage that translate into observable trends in proton-active functional groups on the cell surface. These findings are important for understanding the binding of trace metals to microbes within a thermodynamic framework. For example, surface complexation models have been used to quantify metal adsorption to bacteria over the past two decades (Fein et al., 1997; Cox et al., 1999; Fein and Delea, 1999; Daughney et al., 2001; Yee et al., 2004; Fein et al., 2005; Alessi et al., 2010; Liu et al., 2015). These models use mass action expressions to describe the distribution of metals in experimental systems after equilibrium has been achieved, including the adsorption of protons and dissolved metal species to discrete types of surface functional groups (e.g., carboxyl, phosphoryl and amine). In our past work (Liu et al., 2015), the adsorption of protons and Cd^{2+} to functional groups on the cell wall of *Synechococcus* was described by the following general reactions

$$R\text{-}L_n^- + H^+ \leftrightarrow R\text{-}L_nH^0 \quad (2)$$

$$R\text{-}L_n^- + Cd^{2+} \leftrightarrow R\text{-}L_nCd^+ \quad (3)$$

where L_n^- describes a discrete proton-active bacterial cell wall functional group to which metal species such as Cd^{2+} can bind. The properties of these functional groups, such as their concentrations, densities, and respective protonation constants (pKa), have a direct influence on the potential of those cells to adsorb metals from solution. The substantial changes in cell surface chemistry we observe as a function of nutrition, indicate that the extent to which *Synechococcus* and other marine microorganisms adsorb metal may be substantially impacted by variations in the chemistry of the seawater in

which they grow.

There are strong reasons to believe that the observed relationships between cyanobacterial cell surface reactivity and nutrient regime would be similarly expressed in the marine realm. Relatively small differences in nutrient utilization or regional adaptation in cyanobacteria translates into biochemical responses that are reflected in variations in elemental composition of the cells. P quotas for marine cyanobacteria have been reported to vary over approximately an order of magnitude (e.g., 22–116 amol/cell; Heldal et al., 2003; Twining et al., 2010), consistent with the suggestion that cyanobacteria possess radical surface modification mechanisms to cope with nutrient limitation, such as replacement of surface phospholipids with sulfolipids (Van Mooy et al., 2006). In our study, we observed a decreased role for protein in cell surface reactivity, and increased role for carbohydrates and lipids, as media N:P ratios departed from the reference condition of 14.5. This appears to mirror observations from the marine realm, where gross protein production by bacterioplankton (as measured by leucine incorporation) has been observed to decrease from oligotrophic offshore settings (where it is maximal) to mesotrophic near-shore settings (e.g., in the sub-tropical Atlantic ocean; Hoppe et al., 2006). Our finding that shifts in nutrient and growth regimes yields important surface compositional modifications is consistent with the emerging view of compositional plasticity amongst marine cyanobacteria, and crucially, constitutes the first evidence that such modifications may be expressed in the physico–chemical properties of the cyanobacterial cell surface – and thus in it's capacity to sequester metals from marine

waters by adsorption and co-precipitation processes.

5. CONCLUSIONS

The concentration of protein-related amine groups, lipids and LPS-related carboxyl groups associated with *Synechococcus* cell surfaces varied significantly under different growth conditions. The nitrogen metabolic pathway and phosphorus composition of the growth medium were greater determinants of ligand variability than growth phase. These results support the idea that the *Synechococcus* surface is a dynamic interface where cell wall structure and composition adjust in response to nutritional or environmental conditions over short timescales. The results of this study also have great implications for biological metal cycling in the ocean's photic zone. In a previous study, Liu et al. (2015) suggested that the ability of *Synechococcus* to adsorb dissolved cadmium from seawater implies that it could be an underappreciated driver for the transfer of metal cations from the water column to the seafloor. This present study shows that nutrient-induced variations in surface charge will impact the propensity of *Synechococcus* cells to adsorb solutes in differing marine settings.

ACKNOWLEDGEMENTS

The authors would like to thank the assistance with the FT-IR analyses in the Department of Chemistry Analytical and Instrumentation Laboratory, University of Alberta (Wayne Moffat). This work was supported by Natural Science and Engineering Research Council (NSERC) grants to KOK, DSA and GWO. SVL acknowledges financial support from

LabexMER.

References

Acharya, C., Joseph, D., Apte, S. 2009. Uranium sequestration by a marine cyanobacterium, *Synechococcus* elongatus strain BDU/75042. *Bioresour. Technol.* **100**(7): 2176-2181.

Ahlgren, N. A., Rocap, G. 2012. Diversity and Distribution of Marine Synechococcus: Multiple gene phylogenies for consensus classification and development of qPCR assays for sensitive measurement of clades in the ocean. *Front. Microbio.* **3**(213): 1-24.

Alessi, D.S., Henderson, J.M., Fein, J.B. 2010. Experimental measurement of monovalent cation adsorption onto Bacillus subtilis cells. *Geomicrobiol. J.* **27**(5): 464-472.

Alessi, D.S., Lezama-Pacheco, J.S., Stubbs, J.E., Janousch, M., Bargar, J.R., Persson, P., Bernier-Latmani, R. 2014. The product of microbial uranium reduction includes multiple species with U(IV)-phosphate coordination. *Geochim. Cosmochim. Acta* **131**(15): 115-127.

Baines, S. B., Twining, B. S., Brzezinski, M. A., Krause, J. W., Vogt, S., Assael, D., McDaniel, H. 2012. Significant silicon accumulation by marine picocyanobacteria. *Nat. Geosci.* **5**(12): 886–891.

Baughman, G.L., Paris, D.F., Hodson, R.E. 1981. Microbial bioconcentration of organic pollutants from aquatic systems - a critical review. *Crit. Rev. Microbiol.* **8**(3): 205-228.

Benning, L.G., Phoenix, V., Yee, N., Konhauser, K. 2004. The dynamics of cyanobacterial silicification: an infrared micro-spectroscopic investigation. *Geochim. Cosmochim. Acta* **68**(4): 743-757.

Beveridge, T., Forsberg, C., Doyle, R. 1982. Major sites of metal binding in *Bacillus licheniformis* walls. *J. Bacteriol.* **150**(3): 1438-1448.

Boonaert, C.J., Rouxhet, P.G. 2000. Surface of lactic acid bacteria: relationships between chemical composition and physicochemical properties. *Appl. Environ. Microbiol.* **66**(6): 2548-2554.

Borrok, D., Fein, J., Tischler, M., O'loughlin, E., Meyer, H., Liss, M., Kemner, K. 2004. The effect of acidic solutions and growth conditions on the adsorptive properties of bacterial surfaces. *Chem. Geol.* **209**(1): 107-119.

Boyanov, M.I., Kelly, S.D., Kemner, K.M., Bunker, B.A., Fein, J.B., Fowle, D.A., 2003. Adsorption of cadmium to *Bacillus subtilis* bacterial cell walls: a pH-dependent X-ray absorption fine structure spectroscopy study. *Geochim. Cosmochim. Acta* **67**(18): 3299-3311.

Bruinsma, G.M., Rustema-Abbing, M., van der Mei, H.C., Busscher, H.J. 2001. Effects of cell surface damage on surface properties and adhesion of *Pseudomonas aeruginosa*. *J. Microbiol. Methods* **45**(2): 95-101.

Castro, F.D., Sedman, J., Ismail, A.A., Asadishad, B., Tufenkji, N. 2010. Effect of dissolved oxygen on two bacterial pathogens examined using ATR-FTIR spectroscopy, microelectrophoresis, and potentiometric titration. *Environ. Sci. Technol.* **44**(11): 4136-4141.

Castro, F.D., Tufenkji, N. 2007. Relevance of nontoxigenic strains as surrogates for *Escherichia coli* O157: H7 in groundwater contamination potential: role of temperature and cell acclimation time. *Environ. Sci. Technol.* **41**(12): 4332-4338.

Chen, M., Wang, W.X. 2008. Accelerated uptake by phytoplankton of iron bound to humic acids. *Aquat. Biol.* **3**(2), 155-167.

Clarke, W.A., Konhauser, K.O., Thomas, J.C., Bottrell, S.H. 1997. Ferric hydroxide and ferric hydroxysulfate precipitation by bacteria in an acid mine drainage lagoon. *FEMS Microbiol. Rev.* **20**(3-4): 351-361.

Colica, G., Mecarozzi, C.P., De Philippis, R. 2010. Treatment of Cr(IV)-containing wastewaters with exopolysaccharide-producing cyanobacteria in pilot flow through and batch systems. *Appl. Microbiol. Biotechnol.* **87**(5): 1953-1961.

Collier, J.L., Lovindeer, R., Xi Y., Radway, J.C., Armstrong, R.A. 2012. Differences in growth and physiology of marine *synechococcus* (cyanobacteria) on nitrate versus ammonium are not determined solely by nitrogen source redox state. *J. Phycol.* **48**(1): 106-116

Cox, J.S., Smith, D.S., Warren, L.A., Ferris, F.G. 1999. Characterizing heterogeneous bacterial surface functional groups using discrete affinity spectra for proton binding. *Environ. Sci. Technol.* **33**(24): 4514-4521.

Daughney, C.J., Fowle, D.A., Fortin, D. 2001. The effect of growth phase on proton and metal adsorption by *Bacillus subtilis*. *Geochim. Cosmochim. Acta* **65**(7): 1025-1035.

De Philippis, R., Colica, G., Micheletti, E. 2011. Exopolysaccharide-producing cyanobacteria in heavy metal removal from water: molecular basis and practical applicability of the biosorption process. *Appl. Microbiol. Biotechnol.* **92**(4), 697-709.

Deutsch, C., Weber, T. 2012. Nutrient ratios as a tracer and driver of ocean biogeochemistry. *Ann. Rev. Mar. Sci.* **4**(8), 113-141.

Diem, M. 1993. Introduction to modern vibrational spectroscopy. Wiley New York.

Dittrich, M., Sibler, S. 2005. Cell surface groups of two picocyanobacteria strains studied by zeta potential investigations, potentiometric titration, and infrared spectroscopy. *J. Colloid Interface Sci.* **286**(2): 487-494.

Ede, S.M., Hafner, L.M., Fredericks, P.M. 2004. Structural changes in the cells of some bacteria during population growth: a fourier transform infrared–attenuated total reflectance study. *Appl. Spectrosc.* **58**(3): 317-322.

Falkowski, P.G. 1997. Evolution of the nitrogen cycle and its influence on the biological sequestration of CO_2 in the ocean. *Nature*, **387**(6630): 272-275.

Fein, J.B., Daughney, C.J., Yee, N., Davis, T.A. 1997. A chemical equilibrium model for metal adsorption onto bacterial surfaces. *Geochim. Cosmochim. Acta* **61**(16): 3319-3328.

Fein, J.B., Delea, D. 1999. Experimental study of the effect of EDTA on Cd adsorption by *Bacillus subtilis*: a test of the chemical equilibrium approach. *Chem. Geol.* **161**(4): 375-383.

Fein,J.B., Boily, J.F., Yee, N., Gorman-Lewis, D., Turner, B.F. 2005. Potentiometric titrations of *Bacillus subtilis* cells to low pH and a comparison of modeling approaches. *Geochim. Cosmochim. Acta* **69**(5): 1123-1132.

Felten, J., Hall, H., Jaumot, J., Tauler, R., Juan, A.d., Gorzsas, A. 2015. Vibrational spectroscopic image analysis of biological material using multivariate curve resolution-alternationg least squares (MCR-ALS). *Nature Protoc.* **10**(2): 217-240.

Flombaum, P., Gallegos, J.L., Gordillo, R.A., Rincón, J., Zabala, L.L., Jiao, N., Karl, D.M., Li, W.K., Lomas, M.W., Veneziano, D. 2013. Present and future global distributions of the marine Cyanobacteria

Prochlorococcus and *Synechococcus*. *Proc. Natl. Acad. Sci. USA* **110**(24): 9824-9829.

Foster, J.S., Singh, A.K., Rothschild, L.J., Sherman, L.A. 2007. Growth-phase dependent differential gene expression in *synechocystis* sp strain pcc 6803 and regulation by a group 2 sigma factor. *Arch. Microbiol.* **187**(4): 265-279.

Haas, J.R. 2004. Effects of cultivation conditions on acid–base titration properties of *Shewanella putrefaciens*. *Chem. Geol.* **209**(1): 67-81.

Hancock, I.C. 1991. Microbial cell surface architecture. *Microbial cell surface analysis: structural and physicochemical methods*. 23-59.

Heldal, M., Scanlan, D.J., Norland, S., Thingstad, F., Mann, N.H. 2003. Elemental composition of single cells of various strains of marine *Prochlorococcus* and *Synechococcus* using X-ray microanalysis. *Limnol. Oceanogr.* **48**(5): 1732-1744.

Hennig, C., Panak, P.J., Reich, T., Roβberg, A., Raff, J., Selenska-Pobell, S., Matz, W., Bucher, J.J., Bernhard, G., Nitsche, H. 2001. EXAFS investigation of uranium(VI) complexes formed at *Bacillus cereus* and *Bacillus subtilis* surfaces. *Radiochim. Acta* **89**(10): 625-631.

Herbelin, A.L., Westall, J.C. 1999. FITEQL 4.0: A computer program for determination of chemical eqilibrium constants from experimental data.

Herrero, A., Muro-pastor, A.M., Flores, E. 2001. Nitrogen control in cyanobacteria. *J Bacteriol.* **183**(2): 411-425.

Hong, Y., Brown, D.G. 2006. Cell surface acid–base properties of *Escherichia coli* and *Bacillus brevis* and variation as a function of growth phase, nitrogen source and C:N ratio. *Colloids Surf. B Biointerfaces* **50**(2): 112-119.

Hoppe, H. G., Gocke, K., Koppe, R., Kraus, G. 2006. Changing bacterioplankton growth characteristics on a large spatial scale: oligotrophic versus mesotrophic ocean. *Mar. Ecol. Prog. Ser.* **323**: 21–33.

Howarth, R.W. 1988. Nutrient limitation of net primary production in marine ecosystems. *Annu. Rev. Ecol. System* **19**: 89-110.

Huisman, G., Siegele, D., Zambrano, M., Kolter, R. 1996. Morphological and physiological changes during stationary phase. *Escherichia coli* and *Salmonella: cellular and molecular biology* **2**: 1672-1682.

Jiang, W., Saxena, A., Song, B., Ward, B.B., Beveridge, T.J., Myneni, S.C. 2004. Elucidation of functional groups on gram-positive and gram-negative bacterial surfaces using infrared spectroscopy. *Langmuir*, **20**(26): 11433-11442.

Johnson, Z.I., Zinser, E.R., Coe, A., McNulty, N.P., Woodward, E.M.S., Chisholm, S.W. 2006. Niche partitioning among *Prochlorococcus* ecotypes along ocean-scale environmental gradients. *Science* **311**(5768): 1737–1740.

Kansiz, M., Heraud, P., Wood, B., Burden, F., Beardall, J., McNaughton, D. 1999. Fourier transform infrared microspectroscopy and chemometrics as a tool for the discrimination of cyanobacterial strains. *Phytochemistry*, **52**(3): 407-417.

Kenney, J.P.L., Song, Z., Bunker, B.A., Fein, J.B. 2012. An experimental study of Au removal from solution by non-metabolizing bacterial cells and their exudates. *Geochim. Cosmochim. Acta* **87**(15): 51-60.

Kong, J., Yu, S. 2007. Fourier transform infrared spectroscopic analysis of protein secondary structures. *Acta Biochim. Biophys. Sin.* **39**(8): 549-559.

Konhauser, K.O., Fisher, Q.J., Fyfe, W.S., Longstaffe, F.J., Powell, M.A. 1998. Authigenic mineralization and

detrital clay binding by freshwater biofilms: the Brahmani River, India. *Geomicrobiol. J.* **15**(3): 209-222.

Konhauser, K.O. 2007. Introduction to Geomicrobiology. Blackwell Publishing, Oxford, UK.

Lalonde, S., Smith, D., Owttrim, G., Konhauser, K. 2008a. Acid–base properties of cyanobacterial surfaces I: influences of growth phase and nitrogen metabolism on cell surface reactivity. *Geochim. Cosmochim. Acta* **72**(5): 1257-1268.

Lalonde, S., Smith, D., Owttrim, G., Konhauser, K. 2008b. Acid–base properties of cyanobacterial surfaces. II: silica as a chemical stressor influencing cell surface reactivity. *Geochim. Cosmochim. Acta* **72**(5): 1269-1280.

Leone, L., Ferri, D., Manfredi, C., Persson, P., Shchukarev, A., Sjöberg, S., Loring, J. 2007. Modeling the acid-base properties of bacterial surfaces: a combined spectroscopic and potentiometric study of the gram-positive bacterium *Bacillus subtilis*. *Environ. Sci. Technol.* **41**(18): 6465-6471.

Liu, Y., Alessi, D.S., Owttrim, G.W., Petrash, D.A., Mloszewska, A.M., Lalonde, S.V., Martinez, R.E., Zhou, Q., Konhauser, K.O. 2015. Cell surface reactivity of *Synechococcus* sp. PCC 7002: implications for metal sorption from seawater. *Geochim. Cosmochim. Acta* **169**(15): 30-44.

Lomas, M.W., Bonachela, J.A., Levin, S.A., Martiny, A.C. 2014. Impact of ocean phytoplankton diversity on phosphate uptake. *Proc. Natl. Acad. Sci. USA* **111**(49): 17540-11754.

Mérida, A., Candau, P., Florencio, F.J. 1991. Regulation of glutamine synthetase activity in the unicellular cyanobacterium *Synechocystis* sp. strain PCC 6803 by the nitrogen source: effect of ammonium. *J. Bacteriol.* **173**(13): 4095-4100.

Madigan, M.T., Martinko, J.M., Dunlap, P.V., Clark, D.P. 2008. Brock Biology of microorganisms 12th edn.

Malouin, F., Chamberland, S., Brochu, N., Parr, T. 1991. Influence of growth media on *Escherichia coli* cell composition and ceftazidime susceptibility. *Antimicrob. Agents Chemother.* **35**(3): 477-483.

Meade, A.D., Lyng, F.M., Knief, P., Byrne, H.J. 2007. Growth substrate induced functional changes elucidated by FTIR and raman spectroscopy in in–vitro cultured human keratinocytes. *Anal. Bioanal. Chem.* **387**(5): 1717-1728.

Moore, L.R., Post, A.F., Rocap, G., Chisholm, S.W. 2002. Utilization of different nitrogen sources by the marine cyanobacteria prochlorococcus and synechococcus. *Limnol. Oceanogr.* **47**(4**)**: 989-996.

Movasaghi, Z. 2008. Fourier transform infrared (FTIR) spectroscopy of biological tissues. *Appl. Spectrosc. Rev.* **43**(2): 134-179.

Mozes, N., Léonard, A., Rouxhet, P.G. 1988. On the relations between the elemental surface composition of yeasts and bacteria and their charge and hydrophobicity. *Biochim. Biophys. Acta* **945**(2): 324-334.

Omoike, A., Chorover, J. 2004. Spectroscopic study of extracellular polymeric substances from *Bacillus subtilis:* aqueous chemistry and adsorption effects. *Biomacromolecules*, **5**(4): 1219-1230.

Pradhan, S., Singh, S., Rai, L.C. 2007 Characterization of various functional groups present in the capsule of microcystis and study of their role in biosorption of Fe, Ni and Cr. *Bio. Technol.* **98**(3): 595-602.

Quilès, F., Humbert, F., Delille, A. 2010. Analysis of changes in attenuated total reflection FTIR fingerprints of *Pseudomonas fluorescens* from planktonic state to nascent biofilm state. *Spectrochim. Acta A Mol. Biomol. Spectrosc.* **75**(2): 610-616.

Sakamoto, T., Inoue-Sakamoto. K., Bryant, D.A. 1999. A novel nitrate/nitrite permease in the marine

cyanobacterium *Synechococcus* sp. strain PCC 7002. *J Bacteriol.* **181**(23): 7363-7372

Sarret, G., Manceau, A., Spadini, L., Roux, J.C., Hazemann, J.L., Soldo, Y., Eybert-Berard, L., Methonnex, J.J. 1998. Structural determination of Zn and Pb binding sites in *Penicillium chrysogenum* cell walls by EXAFS spectroscopy. *Environ. Sci. Technol.* **32**(11): 1648-1655.

Schuster, K.C., Mertens, F., Gapes, J.R. 1999. FTIR spectroscopy applied to bacterial cells as a novel method for monitoring complex biotechnological processes. *Vib. Spectrosc.* **19**(2): 467-477.

Sohm, J.A., Ahlgren, N.A., Thomson, Z.J., Williams, C., Moffett, J.W., Saito, M.A., Webb, E.A., Rocap, G. 2015. Co-occurring *Synechococcus* ecotypes occupy four major oceanic regimes defined by temperature, macronutrients and iron. *ISME J.* **10**(2): 333–345.

Stevens, S., Van Baalen, C. 1973. Characteristics of nitrate reduction in a mutant of the blue-green alga *Agmenellum quadruplicatum*. *Plant Physiol.* **51**(2): 350-356.

Stevens, S.E., Porter, R.D. 1980. Transformation in *Agmenellum quadruplicatum*. *Proc. Natl. Acad. Sci. USA* **77**(10): 6052-6056.

Stuart, B.H. 1997. The application of Fourier transform raman spectroscopy to polymer tribology. *Spectrochim. Acta A Mol. Biomol. Spectrosc.* **53**(1): 111-118.

Swanner, E.D., Wu, W.F., Hao, L.K., Wüstner, M.L., Obst, M., Moran, D.M., Mcllvin, M.R., Saito, M.A., Kappler, A. 2015. Physiology, Fe(II) oxidation, and Fe mineral formation by a marine planktonic cyanobacterium grown under ferruginous conditions. *Front. Earth Sci.* **3**(60): 1-21.

Twining, B.S., Nunez-Milland, D., Vogt, S., Johnson, R.S., Sedwick, P.N. 2010. Variations in *Synechococcus* cell quotas of phosphorus, sulfur, manganese, iron, nickel, and zinc within mesoscale eddies in the Sargasso sea. *Limnol. Oceanogr.* **55**(2): 492-507.

Tyrrell, T. 1999. The relative influences of nitrogen and phosphorus on oceanic primary production. *Nature*, **400**(6744): 525-531.

van der Mei, H.C., De Vries, J., Busscher, H.J. 2000. X-ray photoelectron spectroscopy for the study of microbial cell surfaces. *Surf. Sci. Rep.* **39**(1): 1-24.

Van Mooy, B.A.S., Rocap, G., Fredricks, H.F., Evans, C.T., Devol, A.H. 2006. Sulfolipids dramatically decrease phosphorus demand by picocyanobacteria in oligotrophic marine environments. *Proc. Natl. Acad. Sci. USA* **103**(23): 8607–8612.

Walker, S.L., Hill, J.E., Redman, J.A., Elimelech, M. 2005. Influence of growth phase on adhesion kinetics of *Escherichia coli* D21g. *Appl. Environ. Microbiol.* **71**(6): 3093-3099.

Wandersman, C., Delepelaire, P. 2004. Bacterial iron sources: from siderophores to hemophores. *Annu. Rev. Microbiol.* **58**: 611-647.

Westall, J.C. 1982. FITEQL: A computer program for determination of chemical equilibrium constants from experimental data. Department of Chem. Oregon State Univ.

Yang, H.-H., Morrow, J.B., Grasso, D., Vinopal, R.T., Smets, B.F. 2006. Intestinal versus external growth conditions change the surficial properties in a collection of environmental *Escherichia coli* isolates. *Environ. Sci. Technol.* **40**(22): 6976-6982.

Yee, N., Benning, L.G., Phoenix, V.R., Ferris, F.G. 2004. Characterization of metal-cyanobacteria sorption reactions: a combined macroscopic and infrared spectroscopic investigation. *Environ. Sci. Technol.* **38**(3): 775-782.

Zeroual, W., Choisy, C., Doglia, S.M., Bobichon, H., Angiboust, J.-F., Manfait, M. 1994. Monitoring of

bacterial growth and structural analysis as probed by FT-IR spectroscopy. *Biochim. Biophys. Acta* **1222**(2): 171-178.

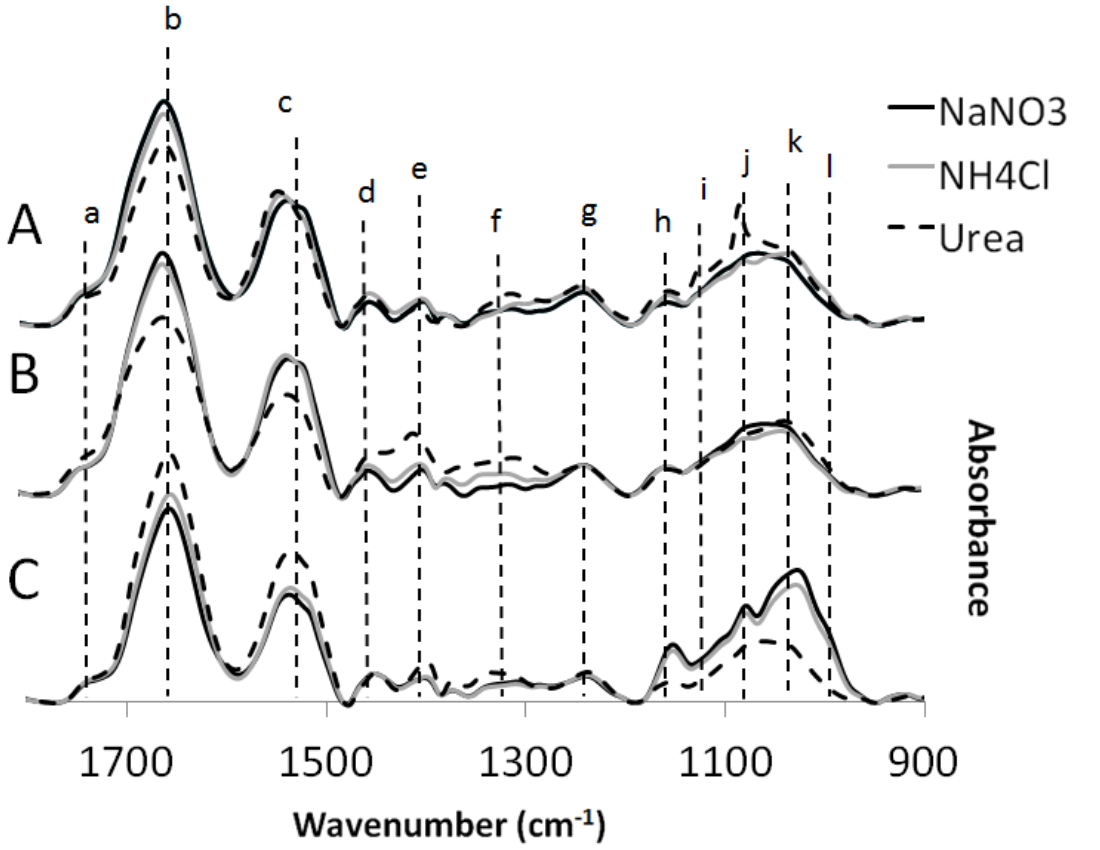

Figure 1. Area normalized FT-IR spectra of *Synechococcus* sp. PCC 7002 obtained from (A) exponential phase, (B) stationary phase, and (C) death phase which acclimated in A+ medium supplemented with either of 17.6 mM nitrate, ammonium or urea as the nitrogen source.

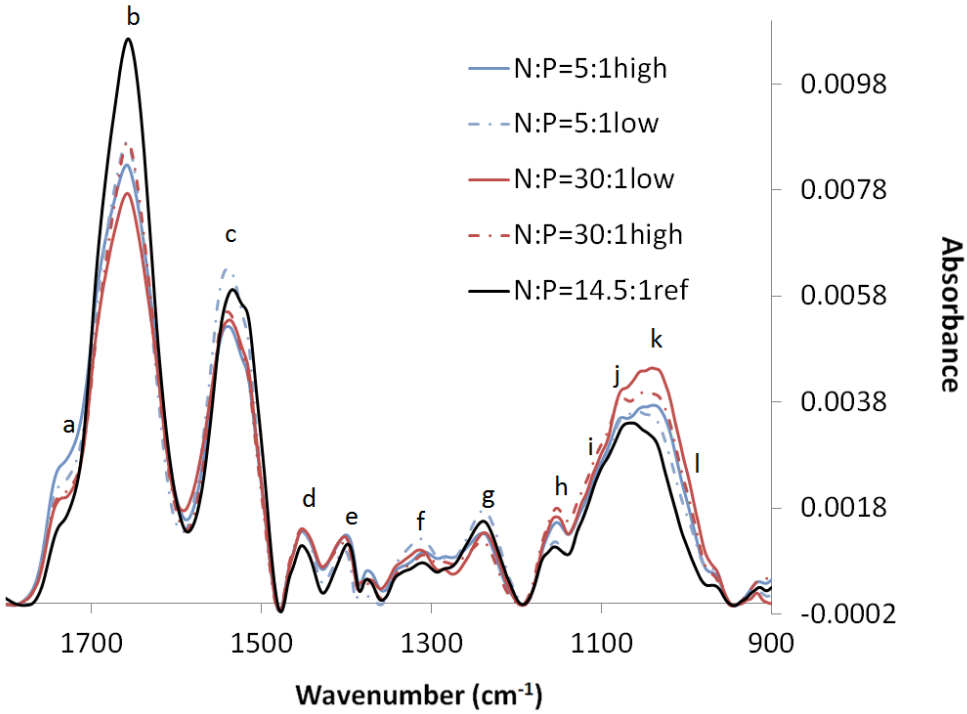

Figure 2. FT-IR spectra of *Synechococcus* sp. PCC 7002 obtained from exponential phase growing in different N:P ratios solutions. $NaNO_3$ served as the N source, and KH_2PO_4 served as the P source.

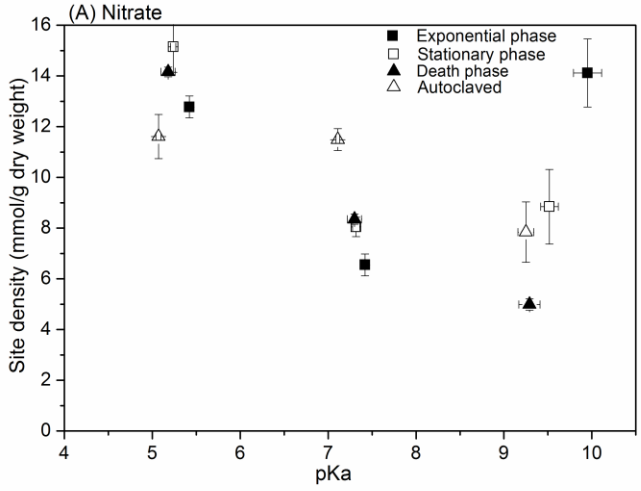

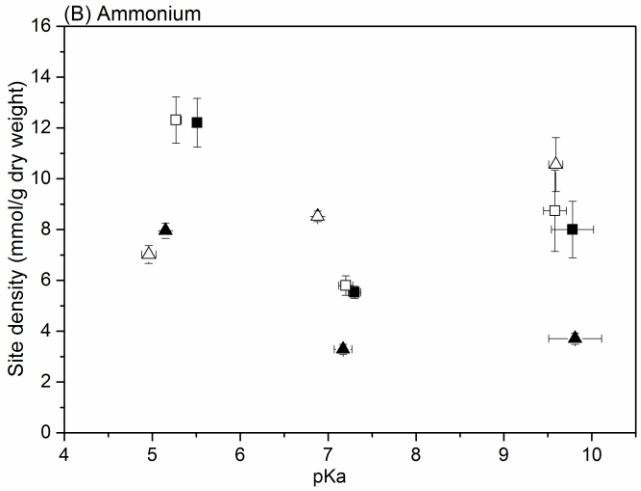

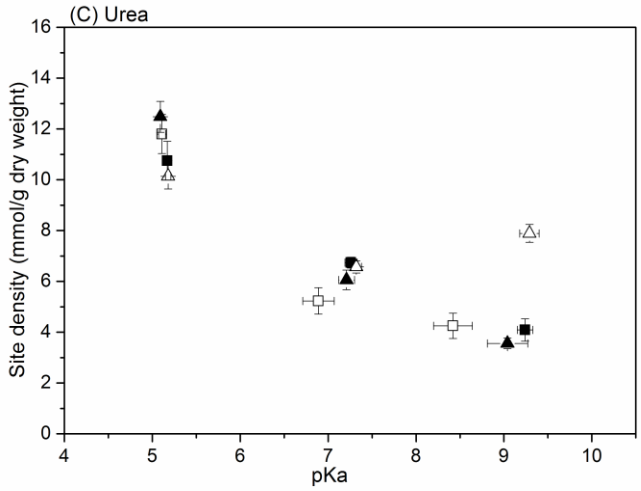

Figure 3. pKa values and their corresponding site concentrations for *Synechococcus* with nitrogen sources of (A) nitrate, (B) ammonium and (C) urea. Error bars represent ±1 standard deviation from a minimum of three titrations.

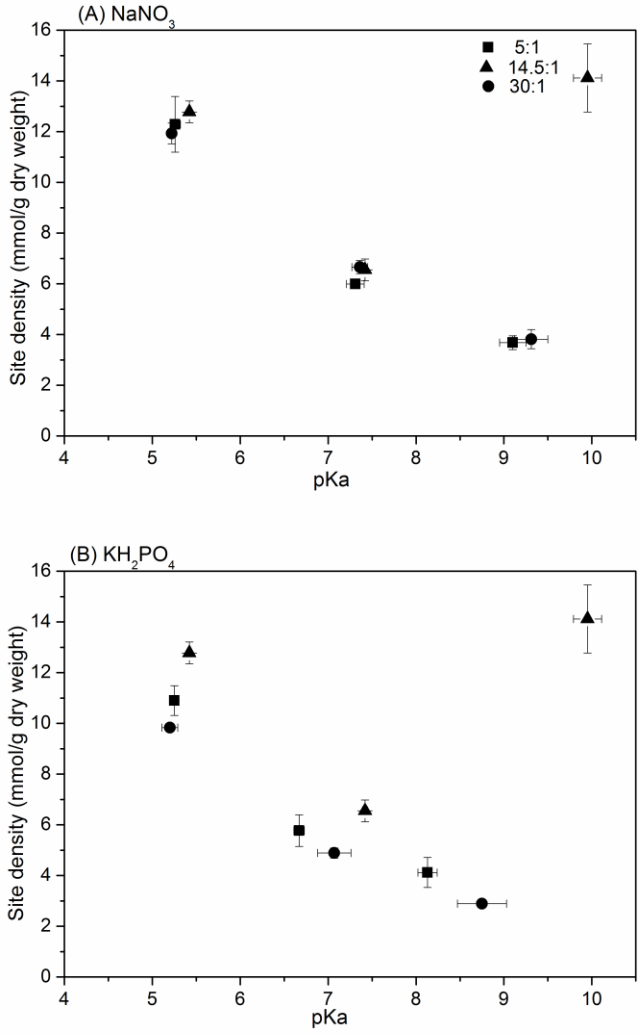

Figure 4. pKa values and their corresponding site concentrations for *Synechococcus* with different nitrogen:phosphate ratios of (A) nitrogen dependent, (B) phosphorus dependent. Error bars represent ±1 standard deviation from a minimum of three titrations.

Table 1. The assignments of principal vibrational bands (compiled after Zeroual et al., 1994; Kansiz et al., 1999; Benning et al., 2004; Jiang et al., 2004; Omoike and Chorover, 2004; Yee et al., 2004; Dittrich and Sibler, 2005; Kong and Yu, 2007; Leone et al., 2007; Meade et al., 2007; Movasaghi et al., 2008; Castro et al., 2010; Quilès et al., 2010; Alessi et al., 2014).

IR band	Wavenumber (cm^{-1})	Functional group assignment
a	1739	V_s C=O of protonated carboxylic acid groups
b	1660	stretching of C=O in amide I, associated with proteins and δO-H of water
c	1537; 1519	N-H bending and C-N stretching in amide II, associated with proteins
d	1455	δ_{as} CH_3 and δ_{as} CH_2 of lipids or proteins
e	1404	$\nu_s COO^-$ from carboxyl groups
f	1351; 1312	δ_s CH_3, νC-N, and δN-H of proteins (amide III) and fatty acids
g	1238	ν_{as} P=O of the phosphodiester backbone of nucleic acid (DNA and RNA), free phosphate, or monoester phosphate functional groups, ν_sC-O of COO- groups
h	1155	ν_sC-OH, νC-O from carbohydrates
i	1105	ν_sP-O-C, ν_{as}C-O-C from phosphate/phosphodiesters and carbohydrates
j	1080	$\nu_s PO_2^-$ of the phosphodiester backbone of nucleic acid (DNA and RNA), or the presence of phosphorylated proteins and polyphosphate storage products
k	1026-1048	Mixed vibrational modes of carbohydrates; $\nu_s PO_2^-$, δC-O-P, ν_sC-OH, νC-O-C, and δ(P-O-P) of polysaccharides
l	1000	νC-O, νC-C from carbohydrates, nucleic acids, or amino acids

ν_s = symmetric stretching; ν_{as} = asymmetric stretching; δ = bending.

Table 2. Modeled pKa distributions and site concentrations (in mmol per g dry cells) for cells grown in different nitrogen sources and growth ages

	pKa_1	pKa_2	pKa_3	$carboxyl_1$	phosphoryl	amine	N_{tot}
Nitrate							
Exponential	5.42(0.03)	7.42(0.03)	9.95(0.16)	12.78(0.43)	6.55(0.43)	14.12(1.34)	34.18(1.62)
Stationary	5.25(0.03)	7.33(0.04)	9.53(0.10)	15.11(1.00)	8.01(0.38)	8.81(1.47)	31.93(1.79)
Death	5.18(0.08)	7.30(0.08)	9.29(0.12)	14.16(0.19)	8.35(0.20)	4.99(0.22)	27.50(0.41)
Autoclaved	5.07(0.03)	7.11(0.02)	9.25(0.09)	11.61(0.87)	11.49(0.43)	7.84(1.19)	30.94(2.27)
Ammonium							
Exponential	5.51(0.04)	7.30(0.07)	9.78(0.24)	12.21(0.96)	5.53(0.24)	8.00(1.11)	25.74(1.51)
Stationary	5.27(0.06)	7.20(0.08)	9.58(0.13)	12.31(0.91)	5.80(0.38)	8.74(1.60)	26.84(1.44)
Death	5.15(0.03)	7.17(0.10)	9.81(0.30)	7.96(0.30)	3.29(0.20)	3.71(0.22)	14.96(0.64)
Autoclaved	4.96(0.08)	6.88(0.02)	9.59(0.08)	7.02(0.35)	8.52(0.21)	10.56(1.06)	26.09(1.42)
Urea							
Exponential	5.17(0.03)	7.26(0.07)	9.24(0.09)	10.75(0.76)	6.74(0.21)	4.09(0.44)	21.57(0.95)
Stationary	5.11(0.04)	6.89(0.18)	8.42(0.22)	11.80(0.77)	5.23(0.52)	4.25(0.50)	21.28(0.69)
Death	5.09(0.02)	7.21(0.09)	9.04(0.23)	12.48(0.61)	6.06(0.39)	3.56(0.21)	22.10(1.01)
Autoclaved	5.18(0.03)	7.32(0.06)	9.29(0.11)	10.14(0.50)	6.57(0.24)	7.89(0.35)	24.60(1.06)

Table 3. Differences of multiple pair-wise comparisons for site density between different nitrogen sources and growth phases

Condition	NO_3^- Exp.	NO_3^- Stat.	NO_3^- Dec.	NH_4^+ Exp.	NH_4^+ Stat.	NH_4^+ Dec.	Urea Exp.	Urea Stat.
Carboxyl site density								
NO_3^- Exp.								
NO_3^- Stat.	**-2.33***							
NO_3^- Dec.	-1.38	0.95						
NH_4^+ Exp.	0.57	**2.90**	**1.95**					
NH_4^+ Stat.	0.47	**2.80****	**1.85**	-0.10				
NH_4^+ Dec.	**4.82**	**7.18**	**6.20****	**4.25****	**4.35****			
Urea Exp.	**2.03****	**4.36**	**3.41**	1.46	1.56	**-2.79**		
Urea Stat.	0.98	**3.31****	**2.36**	0.41	0.51	**-3.84**	-1.05	
Urea Dec.	0.30	**2.63**	1.68	-0.27	-0.17	**-4.52****	**-1.73****	-0.68
Phosphoryl site density								
NO_3^- Exp.								
NO_3^- Stat.	**-1.46****							
NO_3^- Dec.	**-1.80****	-0.34						
NH_4^+ Exp.	**1.02****	**2.48**	**2.82**					
NH_4^+ Stat.	**0.75**	**2.21****	**2.55**	-0.27				
NH_4^+ Dec.	**3.26**	**4.72**	**5.06****	**2.24****	**2.51****			
Urea Exp.	-0.19	**1.27**	**1.61**	**-1.21****	**-0.94**	**-3.45**		
Urea Stat.	**1.32**	**2.78****	**3.12**	0.30	0.57	**-1.94**	**1.51****	
Urea Dec.	0.49	**1.95**	**2.29****	-0.53	-0.26	**-2.77****	0.68	**-0.83***
Amine site density								
NO_3^- Exp.								
NO_3^- Stat.	**5.31****							
NO_3^- Dec.	**9.13****	**3.82****						
NH_4^+ Exp.	**6.12****	0.81	**-3.01**					
NH_4^+ Stat.	**5.38**	0.07	**-3.75**	-0.74				
NH_4^+ Dec.	**10.41**	**5.10**	1.28	**-4.29****	**5.03****			
Urea Exp.	**10.03****	**4.72**	0.90	**3.91****	**4.65**	-0.38		
Urea Stat.	**9.87**	**4.56****	0.74	**3.75**	**4.49****	-0.54	-0.16	
Urea Dec.	**10.56**	**5.25**	1.43	**4.44**	**5.18**	0.15	0.53	0.69
Total site density								
NO_3^- Exp.								
NO_3^- Stat.	2.25							
NO_3^- Dec.	**6.68****	**4.43****						
NH_4^+ Exp.	**8.44****	**6.19**	1.76					
NH_4^+ Stat.	**7.34**	**5.09****	0.66	-1.10				
NH_4^+ Dec.	**19.22**	**16.97**	**12.54****	**10.78****	**11.88****			

Urea Exp.	**12.61****	**10.36**	**5.93**	**4.17****	**5.27**	**-6.61**		
Urea Stat.	**12.90**	**10.65****	**6.22**	**4.46**	**5.56****	**-6.32**	0.29	
Urea Dec.	**12.08**	**9.83**	**5.40****	**3.64**	**4.74**	**-7.14****	-0.53	0.82

Note: Bold represent significant difference. ** comes from significant levels of 0.05 and * comes from significant levels of 0.1.

Table 4. Differences of multiple pair-wise comparisons for site distribution (pka value) between different nitrogen sources and growth phases

Condition	NO_3^- Exp.	NO_3^- Stat.	NO_3^- Dec.	NH_4^+ Exp.	NH_4^+ Stat.	NH_4^+ Dec.	Urea Exp.	Urea Stat.
pKa1								
NO_3^-Exp.								
NO_3^-Stat.	**0.17****							
NO_3^-Dec.	**0.24****	0.07						
NH_4^+ Exp.	-0.09	**-0.26**	**-0.33**					
NH_4^+Stat.	**0.15**	-0.02	-0.09	**0.24****				
NH_4^+Dec.	**0.27**	0.10	0.03	**0.36****	**0.12***			
UreaExp.	**0.25****	0.08	0.01	**0.34****	**0.10**	-0.02		
UreaStat.	**0.31**	**0.14****	0.07	**0.40**	**0.16****	0.04	0.06	
UreaDec.	**0.33**	**0.16**	0.09	**0.42**	**0.18**	0.06	0.08	0.02
pKa2								
NO_3^-Exp.								
NO_3^-Stat.	0.09							
NO_3^-Dec.	0.12	0.03						
NH_4^+ Exp.	0.12	0.03	0.00					
NH_4^+Stat.	**0.22**	0.13	0.10	0.10				
NH_4^+Dec.	**0.25**	0.16	0.13	0.13	0.03			
UreaExp.	0.16	0.07	0.04	0.04	-0.06	-0.09		
UreaStat.	**0.53**	**0.44****	**0.41**	**0.41**	**0.31****	**0.28**	**0.37****	
UreaDec.	0.21	0.12	0.09	0.09	-0.01	-0.04	0.05	**-0.32****
pKa3								
NO_3^-Exp.								
NO_3^-Stat.	**0.42****							
NO_3^-Dec.	**0.66****	0.24						
NH_4^+ Exp.	0.17	-0.25	**-0.49**					
NH_4^+Stat.	0.37	-0.05	**-0.29**	0.20				
NH_4^+Dec.	0.14	-0.28	**-0.52****	-0.03	-0.23			
UreaExp.	**0.71****	0.29	0.05	**0.54***	**0.34**	**0.57**		
UreaStat.	**1.53**	**1.11****	**0.87**	**1.36**	**1.16****	**1.39**	**0.82****	
UreaDec.	**0.91**	**0.49**	0.25	**0.74**	**0.54**	**0.77****	0.20	**-0.62****

Note: Bold represents significant difference. ** comes from significant levels of 0.05 and * comes from significant levels of 0.1.

Table 5 Modeled pKa distributions and site concentrations (in mmol per g dry cells) for cells grown in different N:P ratios

N:P condition	pKa_1	pKa_2	pKa_3	carboxyl	phosphoryl	amine	N_{tot}
14.5:1 reference	5.42(0.03)	7.42(0.03)	9.95(0.16)	12.78(0.43)	6.55(0.43)	14.12(1.34)	34.18(1.62)
30:1 high $NaNO_3$	5.22(0.03)	7.36(0.09)	9.31(0.19)	11.93(0.41)	6.66(0.26)	3.82(0.38)	22.41(0.91)
30:1 low KH_2PO_4	5.20(0.09)	7.07(0.19)	8.75(0.28)	9.83(0.16)	4.89(0.20)	2.89(0.14)	17.61(0.35)
5:1 low $NaNO_3$	5.26(0.06)	7.31(0.10)	9.10(0.15)	12.29(1.10)	5.99(0.16)	3.68(0.27)	21.96(1.35)
5:1 high KH_2PO_4	5.25(0.05)	6.67(0.06)	8.13(0.11)	10.90(0.59)	5.77(0.62)	4.12(0.59)	20.80(0.78)

Table 6. Differences of multiple pair-wise comparisons of site density between different N:P ratios

N:P Condition	N:P=14.5:1	N:P=30:1 high $NaNO_3$	N:P=5:1 low $NaNO_3$	N:P=30:1 low KH_2PO_4	N:P=5:1 high KH_2PO_4
Carboxyl site density					
14.5:1 reference					
30:1 high $NaNO_3$	0.85				
5:1 low $NaNO_3$	0.49	-0.36			
30:1 low KH_2PO_4	**2.95****	**2.10***	**2.46**		
5:1 high KH_2PO_4	**1.88****	1.03	1.39	-1.07	
Phosphoryl site density					
14.5:1 reference					
30:1 high $NaNO_3$	-0.11				
5:1 low $NaNO_3$	0.56	0.67			
30:1 low KH_2PO_4	**1.66****	**1.77***	**1.10**		
5:1 high KH_2PO_4	**0.78***	0.89	0.22	-0.88	
Amine site density					
14.5:1 reference					
30:1 high $NaNO_3$	**10.30****				
5:1 low $NaNO_3$	**10.44****	0.14			
30:1 low KH_2PO_4	**11.23****	0.93	0.79		
5:1 high KH_2PO_4	**10.00****	-0.30	-0.44	-1.23	
Total site density					
14.5:1 reference					
30:1 high $NaNO_3$	**11.77****				
5:1 low $NaNO_3$	**12.22****	0.45			
30:1 low KH_2PO_4	**17.02****	**5.25***	**4.80**		

5:1 high KH_2PO_4	**13.38****	1.61	1.16	**-3.64**

Note: Bold represent significant difference. ** comes from significant levels of 0.05 and * comes from significant levels of 0.1.

Table 7. Differences of multiple pair-wise comparisons for site distribution (pka value) between different N:P ratios

Condition	N:P=14.5:1	N:P=30:1 high $NaNO_3$	N:P=5:1 low $NaNO_3$	N:P=30:1 low KH_2PO_4
pKa1				
N:P=14.5:1 reference				
N:P=30:1 high $NaNO_3$	**0.20****			
N:P=5:1 low $NaNO_3$	**0.16***	-0.04		
N:P=30:1 low KH_2PO_4	**0.22****	0.02	**0.06**	
N:P=5:1 high KH_2PO_4	**0.17****	-0.03	0.01	-0.05
pKa2				
N:P=14.5:1 reference				
N:P=30:1 high $NaNO_3$	0.06			
N:P=5:1 low $NaNO_3$	0.11	0.05		
N:P=30:1 low KH_2PO_4	**0.35****	**0.29***	**0.24**	
N:P=5:1 high KH_2PO_4	**0.75****	0.69	**0.64****	**0.40****
pKa3				
N:P=14.5:1 reference				
N:P=30:1 high $NaNO_3$	**0.64****			
N:P=5:1 low $NaNO_3$	**0.85****	0.21		
N:P=30:1 low KH_2PO_4	**1.20****	**0.56***	0.35	
N:P=5:1 high KH_2PO_4	**1.82****	1.18	**0.97****	**0.62****

Note: Bold represents significant difference. ** comes from significant levels of 0.05 and * comes from significant levels of 0.1.